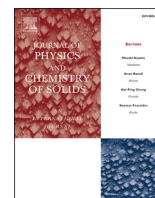




Contents lists available at ScienceDirect

## Journal of Physics and Chemistry of Solids

journal homepage: <http://www.elsevier.com/locate/jpcs>Catalytic activity of Au@Cu<sub>2</sub>O core-shell nanostructure for the organic pollutant remediationSatya Ranjan Jena<sup>a,1</sup>, Bhavya M.B.<sup>a,1</sup>, Sai Rashmi Manippady<sup>a</sup>, Prangya Bhol<sup>a</sup>, Swarnalata Swain<sup>a</sup>, Manav Saxena<sup>a</sup>, Pramila Kumari Misra<sup>b</sup>, Akshaya K. Samal<sup>a,\*</sup><sup>a</sup> Centre for Nano and Material Sciences, Jain University, Ramanagara, Bangalore, 562 112, Karnataka, India<sup>b</sup> Centre of Studies in Surface Science and Technology, School of Chemistry, Sambalpur University, Jyoti Vihar, 768 019, Odisha, India

## ARTICLE INFO

## Keywords:

Au@Cu<sub>2</sub>O  
Core-shell nanostructure  
4-Nitrophenol  
4-Aminophenol  
Dye degradation

## ABSTRACT

Core-shell metal-semiconductor nanostructures have established worldwide interest due to their magnificent chemical, optical and electrical behavior as compared to their monometallic analogous. Wet chemically synthesized gold-copper oxide (Au@Cu<sub>2</sub>O) core-shell nanostructures were studied for catalytic activity for the degradation of dyes such as crystal violet (CV) and congo red (CR) and the reduction of organic pollutant, 4-nitrophenol (4-NP) to 4-aminophenol (4-AP) and compared with Au nanoparticles (Au NPs). The Au@Cu<sub>2</sub>O nanostructures show ten times higher reduction rate for 4-NP than that of monometallic Au NPs. The adsorption followed by degradation of CV, and CR dyes in aqueous solution has been investigated with Au NPs and Au@Cu<sub>2</sub>O core-shell nanostructures. Kinetics study has been performed using Au NPs and Au@Cu<sub>2</sub>O core-shell nanostructure for the 4-NP reduction, CV and CR degradation. The synergistic effect in Au@Cu<sub>2</sub>O core-shell nanostructure facilitates catalytic activity compared to the monometallic Au NPs.

## 1. Introduction

Synthesis of colloidal, single-component metal, and semiconductor nanostructures has increased dramatically from the past two decades [1–4]. Recently, bimetallic nanostructures have considered worldwide attention due to their enhanced properties compared to their monometallic counterparts [5]. The increased attention towards metal-semiconductor nanostructures, such as metal interior-design of anisotropic metal-semiconductor nanostructures [6], different heterodimers and dumbbell-like trimer nanostructures [6,7] and core-shell heteronanostructures have been investigated [8–12]. The appropriate difference in the standard reduction potential is the key factor for the formation of core-shell nanostructures [13]. Cu<sub>2</sub>O is a p-type semiconductor having a band gap of 2.1 eV with interesting excitonic features [14,15] and encompasses unique optoelectronic properties [16] and acts as an excellent photocatalyst [17]. The gold-copper oxide (Au@Cu<sub>2</sub>O) nanostructure is a well-known metal-semiconductor heteronanostructure used for tunable plasmonic properties due to the synergistic effect [18]. Interaction of metal (Au core) and semiconductor (Cu<sub>2</sub>O shell) in Au@Cu<sub>2</sub>O core-shell leads to synergistic effect and enhanced the geometrically tunable optical properties of Au–Cu<sub>2</sub>O core-shell heteronanostructure compared

with Au and Cu<sub>2</sub>O nanoparticles [18]. Au–Cu<sub>2</sub>O core-shell nanostructure showed facet dependent electrical and photocatalytic properties [19]. Su et al. used Au–Cu<sub>2</sub>O core-shell nanostructure on a glassy carbon electrode as a non-enzymatic glucose sensor [20]. Also, Au nanorod embedded Au–Cu<sub>2</sub>O core-shell nanostructure showed excellent photocatalytic performance for methyl orange (MO) degradation [21].

The industrial effluents produced from different industries such as pharmaceutical, textiles and dye industries cause the hazardous issues to humans and environment. 4-Nitrophenol (4-NP), is an important and the key chemical used in various chemical and pharmaceutical industries for the synthesis of pesticides, drugs, and synthetic dyes [22–24]. Exposure to 4-NP produces irritation to the skin, eyes, and also damages the liver and blood cells [25,26]. The reduced product of 4-NP i.e., 4-amino phenol (4-AP) is used in the pharmaceutical industries for the manufacturing of paracetamol, phenacetin, and other products [27,28]. The aromatic amino compound also used for photographic developer, anticorrosion-lubricant, corrosion inhibitor, and dye intermediates [28]. Leishangthem et al. studied the reduction of 4-NP to 4-AP using Au/Ag alloy and Au/Ag core-shell nanostructures [29]. Ag@CeO<sub>2</sub> core-shell nanostructures of the sizes 200–400 nm were used as catalyst for the

\* Corresponding author.

E-mail address: [s.akshaya@jainuniversity.ac.in](mailto:s.akshaya@jainuniversity.ac.in) (A.K. Samal).<sup>1</sup> These authors contributed equally.<https://doi.org/10.1016/j.jpcs.2021.109935>

Received 23 October 2020; Received in revised form 31 December 2020; Accepted 3 January 2021

Available online 27 January 2021

0022-3697/© 2021 Elsevier Ltd. All rights reserved.

reduction of 4-NP to 4-AP which completed in 9 min [30]. Guo et al. synthesized Cu<sub>2</sub>O nanospheres and Cu<sub>2</sub>O/Au nanocomposite and these nanostructures were used as catalysts for the reduction of 4-NP. Cu<sub>2</sub>O/Au nanocomposite exhibited enhanced catalytic activity for the reduction of 4-NP as compared to Cu<sub>2</sub>O nanospheres [31]. It indicates that the bimetallic nanostructures such as nanocomposite, alloy or core-shell nanostructures exhibit outstanding catalytic activity as compared to the monometallic nanoparticles.

In addition to 4-NP, the advancement in the color industries and the discharged organic dyes along with byproducts in various industrial effluents from food, textile, and fashion or cosmetics are the serious threat to the water bodies, and the environment. Crystal violet (CV) is a widely used dye in textile, leather, cosmetics, and printing industries. It is also used in pharmaceutical industries due to the antibacterial, anti-fungal, antitumor properties [32,33]. The CV dye is responsible for skin, eye, and digestive tract irritation and could affect the cornea and conjunctiva of the human body permanently [34]. Mittal et al. have synthesized ZnO nanoparticles doped with Mn used for CV dye degradation [35]. Shende et al. synthesized graphene-Ce-TiO<sub>2</sub> and graphene-Fe-TiO<sub>2</sub> nanocomposites using in-situ ultrasound assisted method and used as catalyst for the degradation of CV [36]. Congo red (CR) dye is used mainly in textile industries, staining in amyloidosis, and the diagnostic process. It causes eye and skin irritation [37]. Zinc oxide nanoparticles synthesized from *Carissa edulis* extract used for the CR dye degradation [38]. Habibi et al. synthesized the ZnO–CdS core-shell nanostructure of average diameter 50 nm used for CR dye degradation in 75 min [39]. An efficient method is required to minimize the waste and toxic byproducts of dyes, to convert hazardous to harmless substances. Different research groups have studied for the treatment of CV and CR using different active materials/techniques. There are different methods such as chemical and biological oxidation/reduction, precipitation, photocatalysis, and electrochemical process used to remove the hazardous substances from the effluents [40]. But these processes are not capable to take out azo dyes completely from the source because of their colour heaviness, constancy, and resistance to degradation.

Herein, we report the synthesis of Au@Cu<sub>2</sub>O core-shell nanostructures using one-step wet chemical method [41] choosing suitable difference in the standard reduction potential. Au acts as a seed for the growth of Au@Cu<sub>2</sub>O nanostructure. This method possesses not a simple combination of individual metal precursors but provides tunable and unique properties to the nanostructure [42]. The catalytic conversion of 4-NP to 4-AP, the core-shell nanostructure provides significant and faster reduction than Au NPs. The synthesized Au@Cu<sub>2</sub>O core-shell nanostructure shows enhanced catalytic activity for the adsorption followed by degradation of dyes such as CV, and CR compared to the monometallic Au NPs. Kinetic studies were performed for 4-NP, CV, and CR with Au@Cu<sub>2</sub>O core-shell nanostructures and Au NPs which are fitted with pseudo first-order or pseudo second-order kinetic.

## 2. Experimental section

### 2.1. Materials and methods

Chloroauric acid (HAuCl<sub>4</sub>·3H<sub>2</sub>O), Copper (II) nitrate trihydrate (Cu(NO<sub>3</sub>)<sub>2</sub>·3H<sub>2</sub>O), Trisodium citrate (Na<sub>3</sub>C<sub>6</sub>H<sub>5</sub>O<sub>7</sub>), Polyvinylpyrrolidone ((C<sub>6</sub>H<sub>9</sub>NO)<sub>n</sub>, PVP K30), Sodium borohydride (NaBH<sub>4</sub>), 4-Nitrophenol (C<sub>6</sub>H<sub>5</sub>NO<sub>2</sub>) were purchased from SD Fine Chemical Limited, India and used without further purification. Hydrazine hydrate (H<sub>4</sub>N<sub>2</sub>·H<sub>2</sub>O, 99 wt %), Crystal violet and Congo red were purchased from Central Drug House, India.

The absorbance study was carried out using PerkinElmer Lambda 365 UV–visible spectrophotometer using a 10 mm quartz cuvette. Field emission scanning electron microscopy (FESEM) images were obtained with the instrument JEOL, Singapore. Transmission electron microscopy (TEM) and high-resolution transmission electron microscopy (HRTEM) measurements were carried out using Thermo Scientific TALOS F200S

G2 (200 KV), FEG, CMOS Camera 4 K × 4 K. Zeta potential and dynamic light scattering (DLS) measurements were performed using Anton Paar Litesizer500 particle size analyzer. Powder X-ray diffraction (PXRD) was obtained by Rigaku X-ray diffraction ultima-IV, Japan, and was recorded over a range of 10–80° with a scan rate of 2 deg. min<sup>-1</sup> using Cu K<sub>α</sub> radiation.

### 2.2. Experimental section

Synthesis of Au@Cu<sub>2</sub>O core-shell nanostructure follows two steps.

I. Synthesis of Au NPs and II. Synthesis of core-shell nanostructure as explained below.

**I. Synthesis of Au NPs:** Chloroauric acid (HAuCl<sub>4</sub>·3H<sub>2</sub>O) is used as a metal precursor and trisodium citrate (Na<sub>3</sub>C<sub>6</sub>H<sub>5</sub>O<sub>7</sub>) is used as the reducing as well as a capping agent for the growth of Au NPs [43]. In brief, 5 mL of chloroauric acid solution (5.0 × 10<sup>-3</sup> M) was added to 90 mL of DI water and the solution was heated until it begins to boil. 5 mL (0.5% w/v) trisodium citrate solution was added to the boiled solution. Upon heating, the colour of the solution changed from pale yellow to wine red. The solution was allowed to cool at room temperature (~27 °C) and continued the stirring for 30 min for the complete growth of the Au NPs. The synthesized Au NPs solution was stored at room temperature. The size of the Au NPs obtained in this method was ~15 ± 5 nm. These Au NPs are used as the core for the synthesis of Au@Cu<sub>2</sub>O core-shell nanostructure.

**II. Synthesis of Au@Cu<sub>2</sub>O core-shell nanostructures:** 50 mL of 0.01 M of Cu(NO<sub>3</sub>)<sub>2</sub>·3H<sub>2</sub>O and 1 g of PVP taken in a beaker and sonicated for 15 min 5 mL of as prepared Au NPs was added followed by the addition of 12 μL of N<sub>2</sub>H<sub>4</sub>·H<sub>2</sub>O (99 wt%) into the reaction mixture. A color change from light blue to light pink was observed after 5 min of stirring which indicates the formation of core-shell nanostructures [40]. The final color of the solution depends upon the amount of Au NPs added. Then, the solution was centrifuged at 5000 rpm for 15 min twice to remove unwanted ions and redispersed in deionized water and stored in a refrigerator (temp. 10 °C). Here, Au@Cu<sub>2</sub>O core-shell nanostructures are formed using 5 mL of Au NPs solution as seed.

### 2.3. Catalytic reduction of 4-NP

The catalytic rate of the Au@Cu<sub>2</sub>O core-shell nanostructure was determined by the chemical reduction of 4-NP to 4-AP. The chemical reaction was performed in a 10 mm quartz cuvette. 2 mL of 4-NP (0.2 mM) taken in a quartz cuvette and aqueous NaBH<sub>4</sub> (0.2 mL, 0.4 M) solution was added to it. The colour of the solution changes from pale yellow to dark yellow. Finally, 50 μL of the Au NPs and Au@Cu<sub>2</sub>O core-shell nanostructures were added to it in two separate cuvettes. The absorbance spectra were measured at different intervals of time using a UV–visible spectrophotometer. Further, the time-dependent reductive conversion is carried out in the presence of Au NPs and Au@Cu<sub>2</sub>O core-shell nanostructures.

### 2.4. Degradation of dyes

Synthesized Au NPs and Au@Cu<sub>2</sub>O core-shell nanostructures were used as the catalysts for the degradation of CV and CR dyes. The catalytic reactions were carried out for the degradation of the dyes using NaBH<sub>4</sub> in water. 2 mL of CV or CR (0.1 mM) taken in a quartz cuvette and 0.2 mL of NaBH<sub>4</sub> (0.5 M) solution was added to it. 100 μL of Au NPs and Au@Cu<sub>2</sub>O core-shell nanostructures were added separately to the reaction mixture. The absorbance of the dye solution was recorded at different time intervals using UV–vis spectrophotometer. Further, the time dependent degradation was carried out in the presence of Au NPs and Au@Cu<sub>2</sub>O core-shell nanostructures.

### 3. Results and discussion

Au@Cu<sub>2</sub>O core-shell nanostructures were prepared by the reduction of Cu(NO<sub>3</sub>)<sub>2</sub> with reducing agent, hydrazine hydrate in the presence of PVP. 5 mL of as prepared Au NPs used as the core to form Au@Cu<sub>2</sub>O core-shell nanostructure. In reaction due course, the resulting Cu<sup>2+</sup> solution color changed from light blue and then light pink upon addition of Au NPs, indicated the core-shell formation. Fig. 1a shows the absorption spectra of Au NPs and Au@Cu<sub>2</sub>O core-shell nanostructures. The Au NPs exhibited surface plasmon resonance (SPR) band at 520 nm due to the interaction of electromagnetic radiation with metal Au NPs, while Au@Cu<sub>2</sub>O core-shell nanostructures showed SPR peaks at 399 nm (Fig. 1a). The blue shift is due to the presence of Au@Cu<sub>2</sub>O core-shell nanostructures [40]. The weak SPR response is dependent on the thickness of Cu<sub>2</sub>O shells encapsulating the Au core and dependent on the core or shell thickness in the core-shell [44]. Fig. 1b shows the PXRD pattern of spherical Au nanospheres and Au@Cu<sub>2</sub>O core-shell nanostructure, respectively. The diffraction peaks at  $2\theta = 32.3, 35.2, 44.1, 48.7, 53.4, 57.9, 61.8, 65.8, 68.0$  and  $74.3^\circ$  corresponds to the planes (110), (111), (200), (202), (211), (202), (220), (221), (310) and (311), respectively, representing cubic phase (JCPDS no: 65-3288, space group: Pn3m (224),  $a = 0.154$  nm) of Cu<sub>2</sub>O nanocrystals [18]. The other diffraction peaks at  $37.7, 44.3, 64.4,$  and  $77.1^\circ$  corresponds to (111), (200), (220), and (311), respectively, representing the Au face-centered cubic structure (JCPDS no: 04-0784, space group: Fm3m (225) and  $a = 0.154$  nm) [40].

The surface morphological characterization using FESEM confirms that the synthesized monodisperse Au NPs are nearly spherical and in the size range of  $15 \pm 5$  nm (Fig. 2a). Fig. 2b shows FESEM images of the synthesized Au@Cu<sub>2</sub>O core-shell nanostructures of particle size of about  $160 \pm 20$  nm. The core-shell nanostructures are monodispersed spherical particles. The size-distribution histogram confirms the uniformity of the particle size (Fig. 2c and d). The particles are homogeneous in size and shape.

TEM images of Au@Cu<sub>2</sub>O core-shell nanostructure is shown in Fig. 3a. TEM images confirmed that the formation of homogeneous spherical core-shell nanostructures. The size of the Au core and Cu<sub>2</sub>O shell are  $20 \pm 5$  nm and  $135 \pm 15$  nm (shell size), respectively. The mean diameter of pure Au NPs is smaller than the diameter of Cu<sub>2</sub>O shell in the core-shell nanostructures. HRTEM images of the Au@Cu<sub>2</sub>O core-shell nanostructure is shown in Fig. 3b. A remarkable change in the contrast between the dark (Au) and lighter (Cu<sub>2</sub>O) region specifying the formation of the Au@Cu<sub>2</sub>O core-shell nanostructures which is further corroborated with the elemental mapping. The inset image in Fig. 3b shows the lattice fringe with an interplanar distance 0.23 nm corresponds to plane (111) of Au core and the lattice fringe with an interplanar distance of 0.24 nm corresponds to the plane (111) of Cu<sub>2</sub>O shell in Au@Cu<sub>2</sub>O nanostructures. The SAED pattern of Au@Cu<sub>2</sub>O core-shell

nanostructure is shown in Figure S1 in the supporting information. The SAED pattern confirms that the Cu<sub>2</sub>O core-shell was polycrystalline in nature. The concentric diffraction rings in Figure S1 were assigned to the (111), (200), (220), and (311) planes, which correspond to the pure cubic phase of Cu<sub>2</sub>O. The SAED patterns are well agreement to the PXRD results (Fig. 1b).

HAADF images of Au@Cu<sub>2</sub>O core-shell nanostructures provide a clear contrast between the Au core and Cu<sub>2</sub>O shell as shown in Fig. 4a. The elemental mapping of Au@Cu<sub>2</sub>O core-shell nanostructures is shown in Fig. 4b-d. The elemental mapping of each element such as Au, Cu, and oxygen present in the core-shell nanostructure are influenced by incoherently scattered electrons as shown in Fig. 4b-d [45].

The high resolution gives an advantage over the detection of back-scattered electrons used to detect materials with a high atomic weight (Z) in a matrix of material with a lower atomic weight. Au provides strong brightness and lighter element copper shows low brightness. Elemental mapping clearly shows the presence of Au, Cu, and O in Au@Cu<sub>2</sub>O core-shell nanostructures. The EDS spectrum of Au@Cu<sub>2</sub>O core-shell nanostructures is shown in Figure S2 (supporting information). Surface charge present on Au NPs and Au@Cu<sub>2</sub>O core-shell nanostructures were measured by zeta potential and shown in Table 1. The zeta potential value of Au NPs shows  $-34.0$  mV due to the presence of negatively charged citrate ions [46] as a capping agent. However, the zeta potential of the Au@Cu<sub>2</sub>O core-shell nanostructure was reduced to  $-8.9$  mV. Au@Cu<sub>2</sub>O core-shell nanostructures possess incipient stability because of lower zeta potential value [47]. In this case, trisodium citrate plays a major role, which inhibits the particle assemblage during the preparation process of Au@Cu<sub>2</sub>O core-shell nanostructures. Dynamic Light Scattering (DLS) shows the hydrodynamic diameter size based on the diffusion of the particles and the aqueous solution. Table 1 shows the hydrodynamic diameter of the Au NPs and Au@Cu<sub>2</sub>O core-shell nanostructures. The hydrodynamic diameter size of Au NPs is about 50–52 nm and core-shell nanostructures show  $230 \pm 5$  nm, respectively. Figure S3 (a, b) shows the hydrodynamic diameter value of Au NPs and Au@Cu<sub>2</sub>O core-shell nanostructures.

#### 3.1. The catalytic activity of 4-NP reduction

The catalytic activity of 4-NP studied using Au NPs and Au@Cu<sub>2</sub>O as catalysts as shown in Fig. 5. The absorption study of 4-NP shows peak maxima at 317 nm at room temperature. A redshift by 83 nm in peak maxima was observed upon addition of NaBH<sub>4</sub> to 4-NP was observed due to the formation of 4-nitrophenolate ion by de-protonation of 4-NP. The color of the solution turns to dark yellow upon generation of the 4-nitrophenolate ion as compared to 4-NP color (pale yellow). This phenolate ion has stable for a few days and the chemical reduction of 4-NP was not occurred without the catalyst [48]. The reaction progress can be described by the hydrogen carrier Au NPs and Au@Cu<sub>2</sub>O

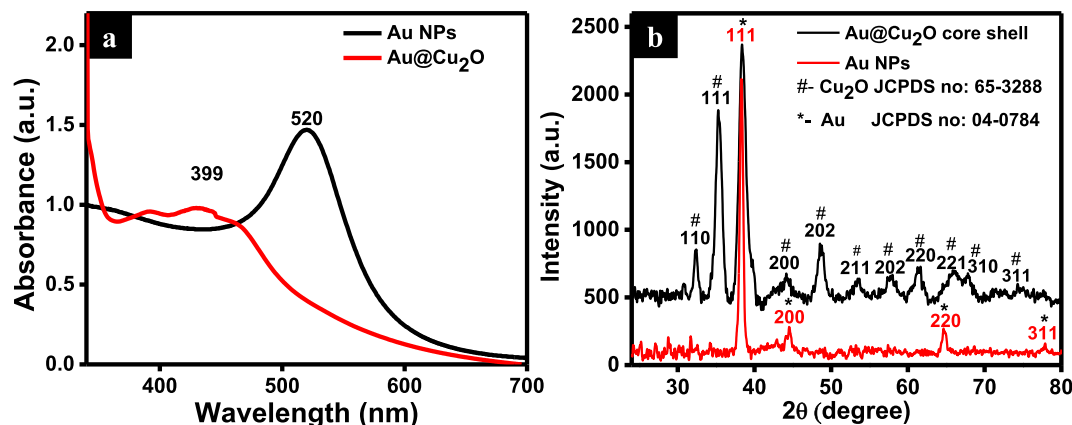


Fig. 1. (a) UV-visible spectra of Au NPs and Au@Cu<sub>2</sub>O core-shell nanostructures, and (b) PXRD pattern of Au@Cu<sub>2</sub>O core-shell nanostructures.

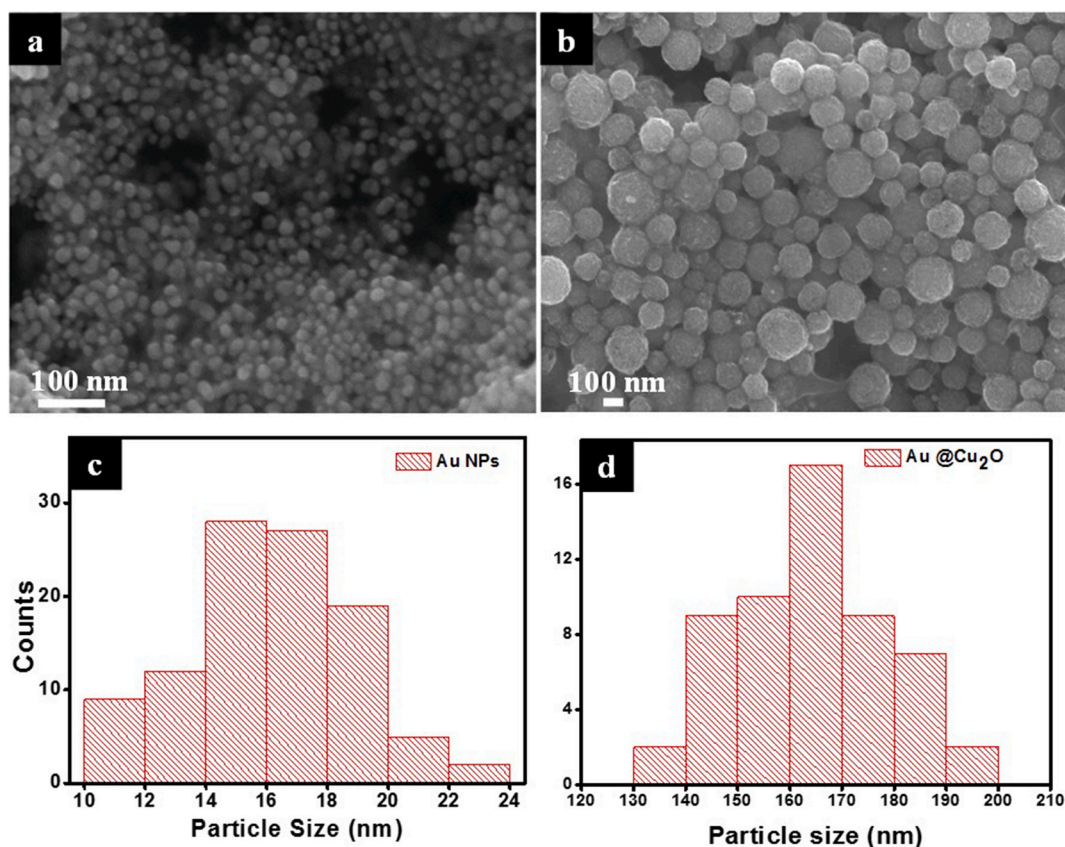


Fig. 2. FESEM morphology of (a) Au NPs, (b) Au@Cu<sub>2</sub>O core-shell nanostructures. (c) and (d) are the particle size distribution of Au NPs and Au@Cu<sub>2</sub>O core-shell nanostructures, respectively.

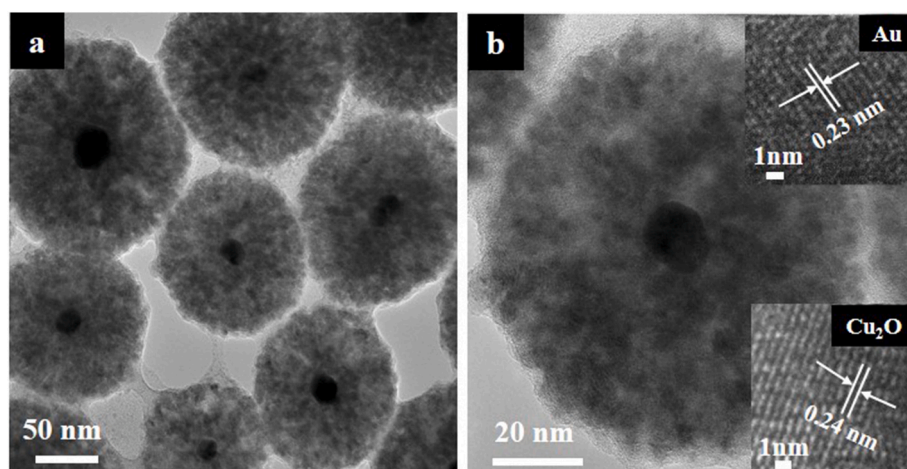


Fig. 3. (a) TEM images of Au@Cu<sub>2</sub>O core-shell nanostructure. (b) HRTEM image of core-shell. Inset of (b) shows the lattice fringes of Au and Cu<sub>2</sub>O, respectively.

core-shell nanostructures which transport the hydrogen from NaBH<sub>4</sub> to 4-NP. Hence, Au NPs and Au@Cu<sub>2</sub>O core-shell nanostructures act as a hydrogen carrier in this chemical reduction reaction [49]. In the solvation reaction of the proton, the normal hydrogen electrode (NHE) is considered as the reference electrode and a thermodynamically possible chemical reaction of 4-NP to 4-AP occurs [50]. However, the interaction of the 4-NP and NaBH<sub>4</sub> shows a slow kinetic reaction [24]. 50  $\mu$ L (8.6 nM) Au@Cu<sub>2</sub>O core-shell nanocatalyst was added to the solution which contains 2 mL of 4-NP and 200  $\mu$ L NaBH<sub>4</sub> (0.4 M). Upon the addition of Au@Cu<sub>2</sub>O core-shell, there was a change in the peak intensity at 400 nm which was gradually decreased with respect to time and simultaneously

gradual increase of a new peak at 300 nm [48], suggest the formation of 4-AP occurred in 4 min. The progress of the chemical reduction was recorded by UV-visible spectrophotometer. 50  $\mu$ L of as prepared Au NPs catalyst is used for the conversion of 4-NP to 4-AP occurs in 40 min as shown in Fig. 5a. In the control reaction, 4-NP reduction by NaBH<sub>4</sub>, there is a slow change in the intensity of 4-nitro phenolate ion at 400 nm due to the slow reduction process. In the absence of a catalyst, there is no change in the phenolate ion peak and also no colour change in the solutions up to 30 min as shown in Figure S4 (supporting information). It was found that the reduction reaction for 4-NP to 4-AP using Au@Cu<sub>2</sub>O core-shell nanostructures was much faster compared to monometallic

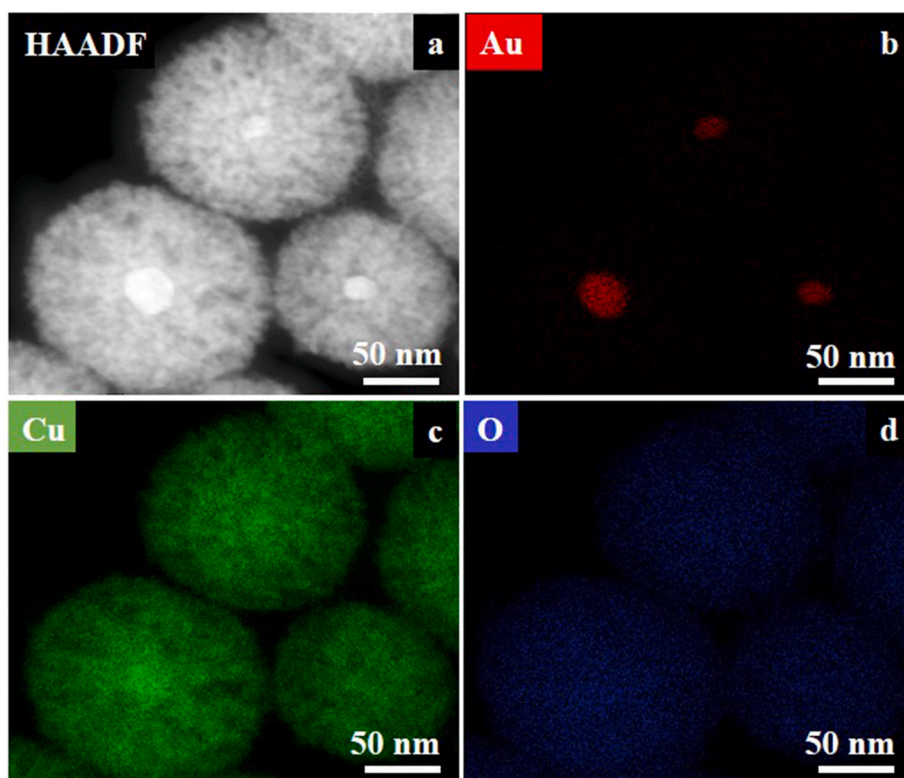


Fig. 4. (a) HAADF-STEM image of the core-shell nanostructure. (b, c, and d) are the elemental analysis of core-shell nanostructures.

**Table 1**

Zeta potential and hydrodynamic diameter value of Au NPs and Au@Cu<sub>2</sub>O core-shell nanostructures.

Sample	Hydrodynamic diameter (nm)	Zeta Potential (mV)
Au NPs	50–52	−34.0
Au@Cu <sub>2</sub> O Core-shell	230 ± 5	−8.9

Au NPs. The reduction process of 4-NP to 4-AP was completed in 40 and 4 min in presence of Au NPs and Au@Cu<sub>2</sub>O, respectively.

The enhanced reduction rate of Au@Cu<sub>2</sub>O core-shell nanostructures may be due to the synergistic effect from the individual components present in Au@Cu<sub>2</sub>O core-shell. The metal (Au core) -semiconductor (Cu<sub>2</sub>O shell) interaction leads plasmonic energy transfer and charge

transfer between Au core and Cu<sub>2</sub>O shell [18,20,51]. Therefore, Au@Cu<sub>2</sub>O core-shell nanostructures are promising catalyst to increase the catalytic activity. Au@Cu<sub>2</sub>O core-shell nanostructure shows 10 times faster reaction rate compared to the Au NPs for the reduction of 4-NP at room temperature. The better catalytic performance of the core-shell nanostructures may be due to the synergistic effect. It shows that the reaction process of 4-NP depends upon the size and constitution of materials in the nanostructures.

### 3.2. Catalytic degradation of dyes

The catalytic degradation of dyes (CV and CR) was carried out using Au NPs and Au@Cu<sub>2</sub>O core-shell nanostructures at room temperature. In this case, NaBH<sub>4</sub> (0.5 M) is used as a reducing agent and the absorption spectra of the dye degradation kinetics was observed by a UV-visible

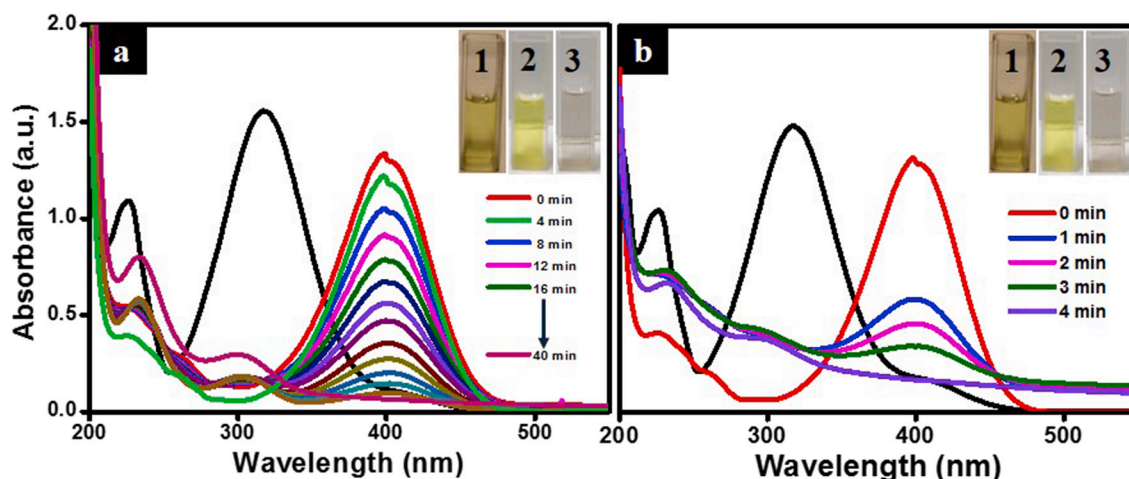


Fig. 5. Reduction of 4-NP using a catalyst (a) 50  $\mu$ L Au NPs, (b) 50  $\mu$ L of Au@Cu<sub>2</sub>O core-shell nanostructures.

spectrophotometer. The UV–visible spectra for CV and CR in aqueous medium show peaks at 594 and 497 nm, respectively. There is no change in absorption peak position, but a slight decrease in the peak intensity upon the addition of  $\text{NaBH}_4$  and constant absorbance observed even after 30 min. Figures S5 and S6 (supporting information) shows that the UV–visible spectra of CV and CR without the addition of a catalyst. The addition of Au NPs and Au@Cu<sub>2</sub>O core-shell nanostructure catalysts separately to CV and CR solution, complete degradation of CV and CR at different time period were observed as shown in Fig. 6. For degradation of CV, 100  $\mu\text{L}$  of each Au NPs and Au@Cu<sub>2</sub>O core-shell nanostructures added separately to the 2.2 mL of dye solution containing CV (2 mL) and  $\text{NaBH}_4$  (0.2 mL). In the case of Au NPs as a catalyst, the complete degradation of dye achieved in 105 min (Fig. 6a), whereas Au@Cu<sub>2</sub>O core-shell nanostructures proceeded faster than Au NPs and took 35 min for the complete degradation of CV (Fig. 6b). 100  $\mu\text{L}$  of each Au NPs and Au@Cu<sub>2</sub>O core-shell nanostructures were used for the degradation of CR. In case of Au NPs as catalyst, complete degradation of dye took 34 min (Fig. 6c) and Au@Cu<sub>2</sub>O core-shell nanostructure shows significant faster results as compared to that of Au NPs. The time required for Au@Cu<sub>2</sub>O core-shell nanostructures was 11 min (Fig. 6d).

The colour change takes place from red to colorless due to the degradation of CR. The mean zeta potential of CV dye is  $-1.3$  mV at pH 3.2 and CR dye shows  $-0.7$  mV at pH 5.9. The zeta potential of Au@Cu<sub>2</sub>O core-shell nanostructure and Au NPs show  $-8.9$  and  $-34.0$  mV, respectively. Due to the low zeta potential of Au@Cu<sub>2</sub>O core-shell nanostructures compared to Au NPs, there is a strong particle–particle interaction between dye and core-shell nanostructure reduces the degradation time compared to Au NPs.

Interaction of core-shell nanostructures with CV and CR are

characterized by FT-IR as shown in Figure S7 and S8 in the supporting information. The CV is a tri-phenyl-methane dye which shows the prominent peak at 3422, 1586, 1361, and 1175  $\text{cm}^{-1}$  [52]. The peak at 1586  $\text{cm}^{-1}$  is assigned to the C=C stretching bond of the benzene ring. Besides, the peak at 1361  $\text{cm}^{-1}$  corresponds to bonding between Ar–N and C–Ar stretching vibrations. The peak at 1175  $\text{cm}^{-1}$  shows the C–N stretching frequency of CV dye. The various peak found between 500 and 1500  $\text{cm}^{-1}$  corresponds to the mono and para di-substituted benzene ring. The core-shell nanostructure shows the peak position at 3416, 1664, and 1385  $\text{cm}^{-1}$ . After the interaction of Au@Cu<sub>2</sub>O core-shell nanostructure with CV, the insignificant peaks were observed at 3467, 1604, and 1356  $\text{cm}^{-1}$ . There is a change of C=C peak which shows at 1604  $\text{cm}^{-1}$  corresponds to the C=O (ketone formation). The CV dye is completely degraded reacting with the Au@Cu<sub>2</sub>O core-shell nanostructure. CR dye is a benzidine-based anionic diazo dye that shows the peaks at 3462, 1604, 1448, 1175, and 1047  $\text{cm}^{-1}$  [53]. The N–H stretching frequency shows at 3462  $\text{cm}^{-1}$  and also the peak at 1604  $\text{cm}^{-1}$  indicates the N=N stretching vibration. The peak at 1448  $\text{cm}^{-1}$  correspond to S=O stretching vibration. The peak at 1047  $\text{cm}^{-1}$  indicates the SO<sub>3</sub>–H bond. Au@Cu<sub>2</sub>O core-shell nanostructure shows peaks at 3421, 2963, 1663, 1383, and 1291  $\text{cm}^{-1}$ . The peak at 2963  $\text{cm}^{-1}$  due to O–H stretching vibration of citrate ion present on the Au NPs [54]. The peak at 3451  $\text{cm}^{-1}$  which indicates the O–H stretching frequency after degradation. There is a decrease in the frequency of N=O shows a peak at 1434  $\text{cm}^{-1}$ . The CR dye is completely degraded in the presence of core-shell nanostructures. The CV and CR dyes are fully degraded using the Au@Cu<sub>2</sub>O core-shell nanostructure as catalyst.

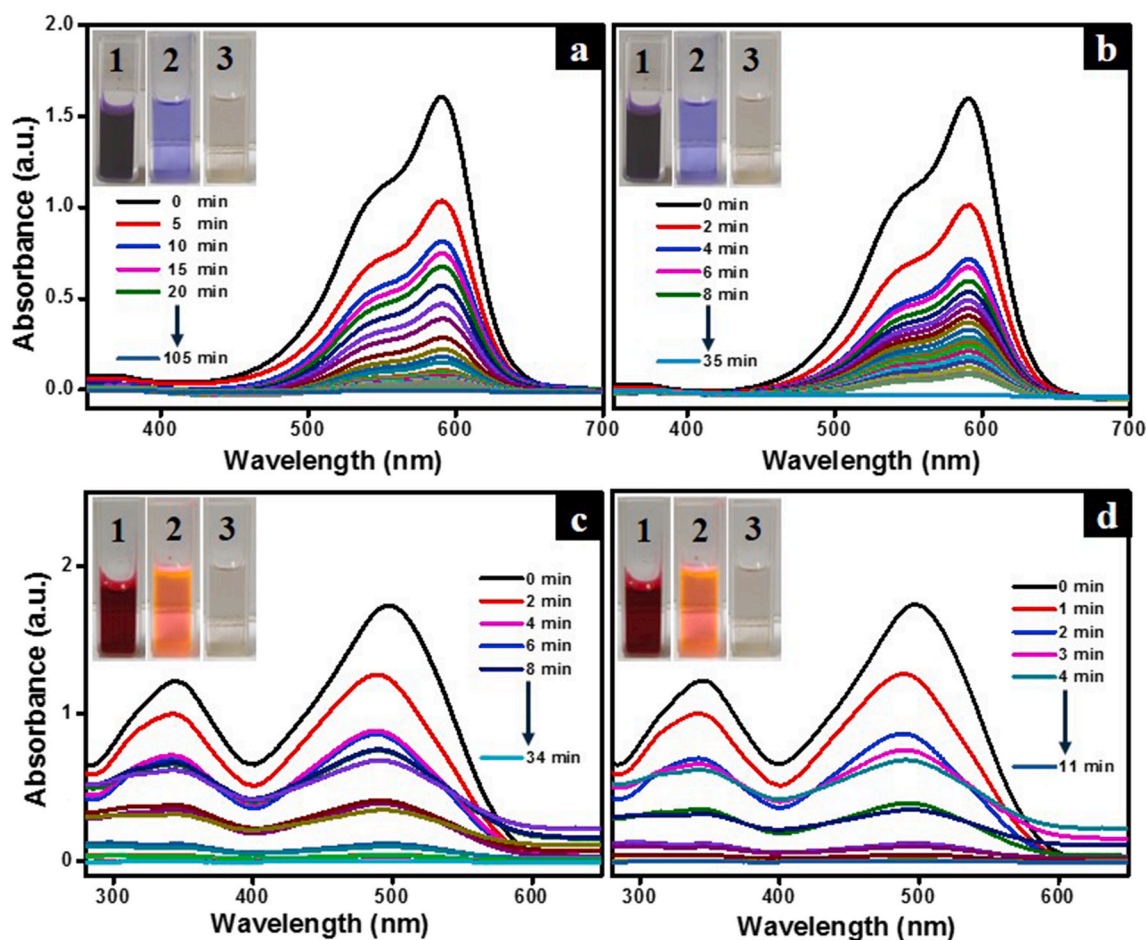


Fig. 6. CV degradation using a catalyst (a) 100  $\mu\text{L}$  Au NPs, (b) 100  $\mu\text{L}$  of Au@Cu<sub>2</sub>O core-shell nanostructures. Congo red degradation using a catalyst (c) 100  $\mu\text{L}$  Au NPs, (d) 100  $\mu\text{L}$  of Au@Cu<sub>2</sub>O core-shell nanostructures.

### 3.3. Kinetic study

To understand the adsorption of 4-NP and dyes, kinetic study was carried out at different time intervals for Au NPs and Au@Cu<sub>2</sub>O core-shell nanostructures.

**For 4-NP:** Kinetics study for 4-NP with Au NPs and Au@Cu<sub>2</sub>O core-shell nanostructures were shown in Fig. 7. For 4-NP adsorption onto Au NP, it is observed that R<sup>2</sup> value of pseudo first-order reaction is 1 (Fig. 7a) and R<sup>2</sup> value of 0.378 for pseudo second-order reaction (Fig. 7b), indicating physisorption. Whereas Au@Cu<sub>2</sub>O core-shell nanostructure shows higher R<sup>2</sup>: 0.952 for pseudo second-order (Fig. 7d) as compared with pseudo first-order R<sup>2</sup>: 0.903 (Fig. 7c), following chemisorption.

**For CV and CR:** For CV dye adsorption onto Au NP, pseudo first-order shows higher correlation coefficient (R<sup>2</sup>: 0.990, Fig. 8a) as compared to pseudo second-order (R<sup>2</sup>: 0.982, Fig. 8b), (Fig. 8a and b) indicating that CV dye follows first-order kinetic and thus follow physisorption process. Whereas, Au@Cu<sub>2</sub>O core-shell nanostructures, pseudo second-order kinetics achieved higher R<sup>2</sup>: 0.985 (Fig. 8d) with that of pseudo first-order kinetics R<sup>2</sup>: 0.969 (Fig. 8c), indicating the chemisorption process. Kinetic study of CR dye onto Au NP is shown in Fig. 8e, where pseudo first-order shows higher R<sup>2</sup>: 0.924 (Fig. 8e) as compared with pseudo second-order R<sup>2</sup>: 0.905 (Fig. 8f), confirming the process of physisorption. However, Au@Cu<sub>2</sub>O core-shell nanostructure shows higher R<sup>2</sup>: 0.898 for pseudo second-order kinetics (Fig. 8h) as compared to pseudo first-order kinetics R<sup>2</sup>: 0.823 (Fig. 8g), following chemisorption.

### 3.4. Recyclability study

Recyclability study of Au@Cu<sub>2</sub>O core-shell nanostructures in dye degradation shown in S9 in the supporting information. The used

catalyst of Au@Cu<sub>2</sub>O core-shell nanostructure was recovered after the reaction and recyclability of the catalyst was studied for the degradation of dyes. The same degradation procedure followed for the recyclability study. First recycles show the recovery of the core-shell nanostructure in CV dye degradation is 82% and CR dye degradation of core-shell nanostructure is 84%. Figure S9 shows that the Au@Cu<sub>2</sub>O core-shell nanostructure catalyst is recyclable up-to four consecutive cycles with greater than 50% of yield (for 4th cycle).

## 4. Conclusion

Au@Cu<sub>2</sub>O core-shell nanostructure is successfully synthesized by wet chemical synthesis method. The synthesized material is used for the catalyst for chemical reduction of 4-NP and catalytic degradation of CV and CR dyes and compared with the parent Au NPs. The core-shell nanostructure shows a higher rate of reduction for 4-NP to 4-AP as compared to the Au NPs. Au@Cu<sub>2</sub>O core-shell nanostructure plays a significant role in the degradation process of CV and CR and shows adsorption followed by degradation activity faster compared to the monometallic Au NPs. The study shows the 4-NP reduction, CV, and CR degradation kinetics are faster, may be due to the synergistic effect between Au and Cu in core-shell nanostructure. Kinetic studies were performed for 4-NP, CV, and CR with Au@Cu<sub>2</sub>O core-shell nanostructures and Au NPs which are fitted with pseudo first-order or pseudo second-order kinetic. Au@Cu<sub>2</sub>O core-shell heteronanostructures are believed to be crucial for other catalytic reactions and industrial dye degradations.

### Author contributions

The manuscript was written through contributions of all authors. All authors have given approval to the final version of the manuscript.

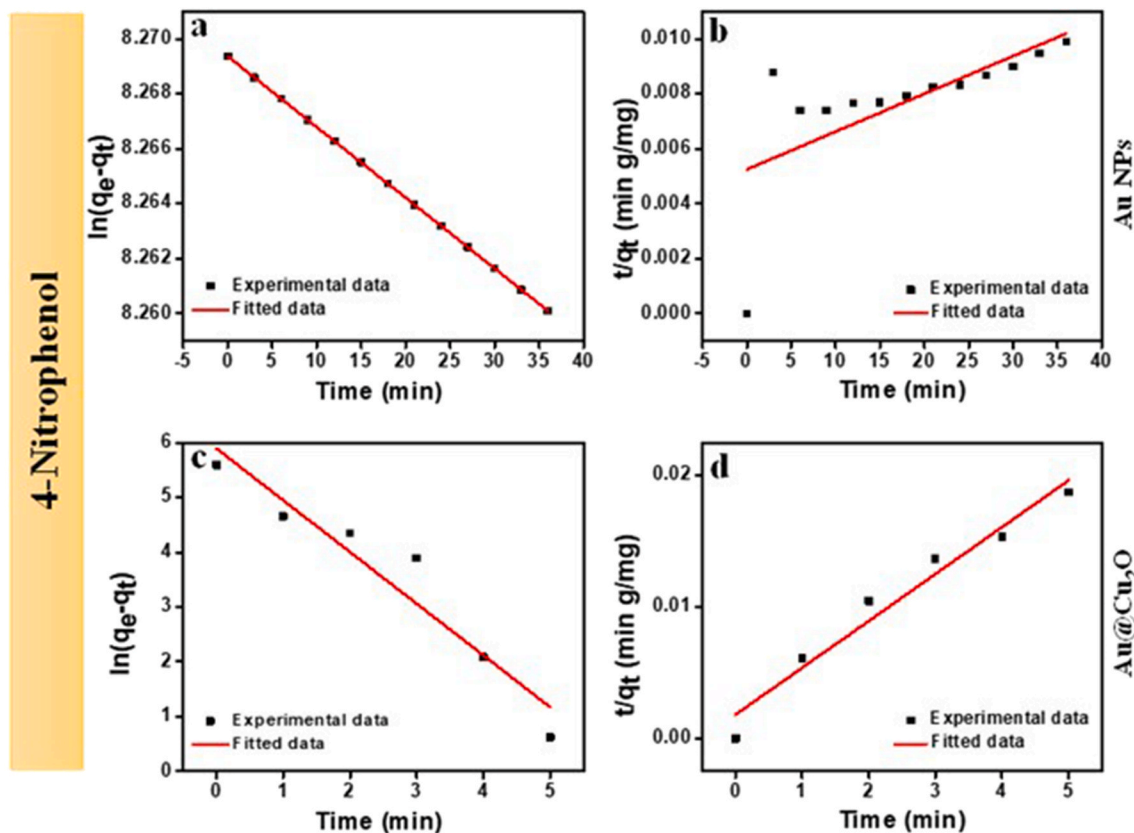
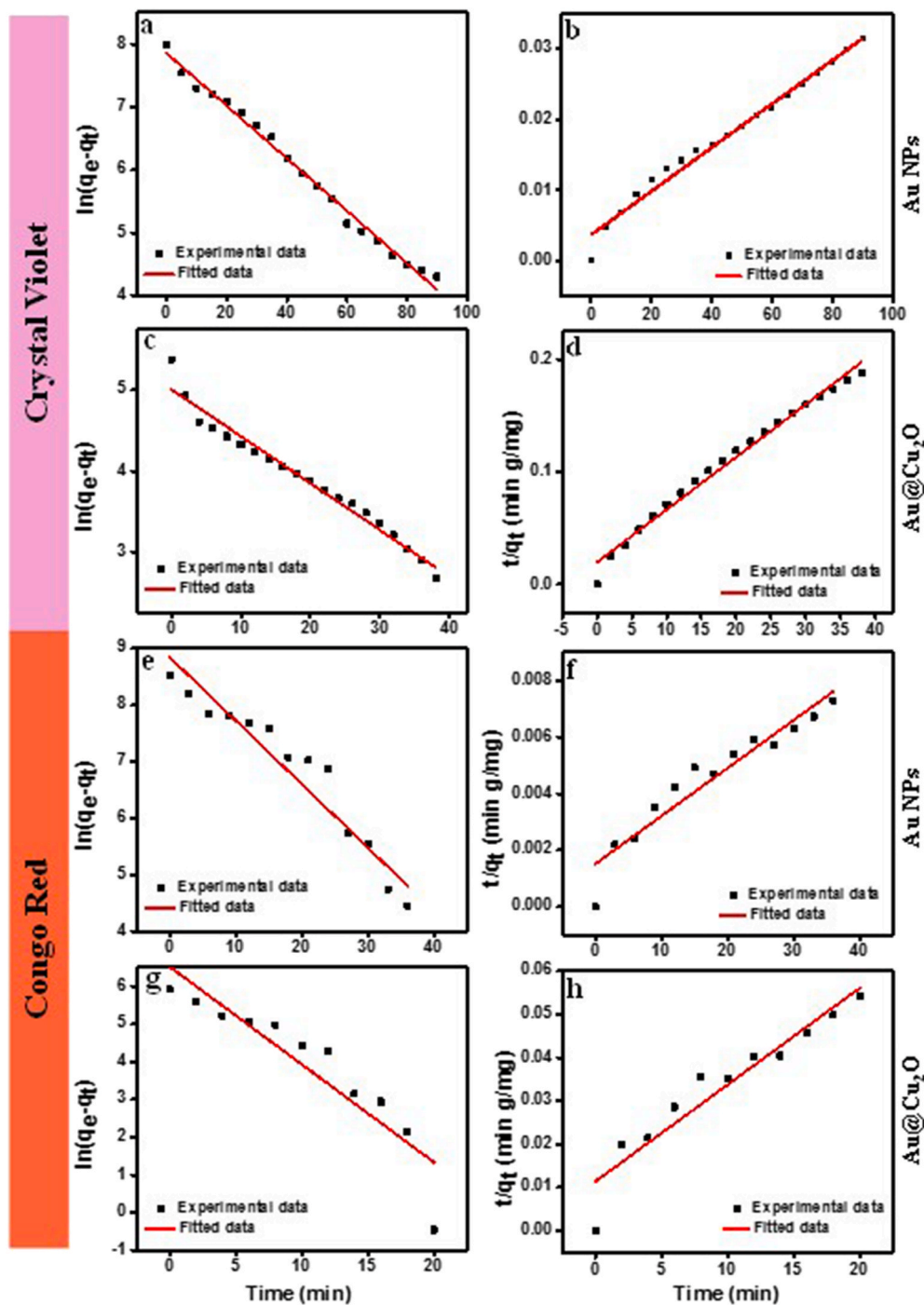


Fig. 7. (a) Pseudo first-order and (b) pseudo second-order kinetics for Au NPs with 4-NP. (c) Pseudo first-order and (d) pseudo second-order kinetics for Au@Cu<sub>2</sub>O core-shell nanostructures with 4-NP.



**Fig. 8.** (a) Pseudo first-order and (b) pseudo second-order kinetics for Au NPs with CV. (c) Pseudo first-order and (d) pseudo second-order kinetics for Au@Cu<sub>2</sub>O core-shell nanostructures with CV. (e) Pseudo first-order and (f) pseudo second-order kinetics for Au NPs with CR. (g) Pseudo first-order and (h) pseudo second-order kinetics for Au@Cu<sub>2</sub>O core-shell nanostructures with CR.

#### CRediT authorship contribution statement

**Satya Ranjan Jena:** Conceptualization, Methodology. **M.B. Bhavya:** Methodology, Writing - original draft, draft preparation. **Sai Rashmi Manippady:** Conceptualization, Formal analysis, data analysis. **Prangya Bhol:** Formal analysis, Writing - original draft, Data analysis, draft editing. **Swarnalata Swain:** Methodology, Writing - original draft, draft editing. **Manav Saxena:** Writing - review & editing, Writing - original draft, Supervision, Reviewing, final drafting. **Pramila Kumari Misra:** Formal analysis, Data analysis, reviewing. **Akshaya K. Samal:** Writing - review & editing, Writing - original draft, Supervision,

Reviewing, final drafting.

#### Declaration of competing interest

The authors declare that they have no known competing financial interests or personal relationships that could have appeared to influence the work reported in this paper.

#### Acknowledgements

SRJ and BMB acknowledges CNMS, JAIN University. AKS is thankful

to the SERB, New Delhi, India for the funding (CRG/2018/003533). The authors thankful to Nano Mission (SR/NM/NS-20/2014) for FESEM and PXRD facility at CNMS, Jain University.

## Appendix A. Supplementary data

Supplementary data to this article can be found online at <https://doi.org/10.1016/j.jpics.2021.109935>.

## References

- [1] C. Burda, X. Chen, R. Narayanan, M.A. El-Sayed, Chemistry and properties of nanocrystals of different shapes, *Chem. Rev.* 105 (2005) 1025–1102.
- [2] M.-C. Daniel, D. Astruc, Gold nanoparticles: assembly, supramolecular chemistry, quantum-size-related properties, and applications toward biology, catalysis, and nanotechnology, *Chem. Rev.* 104 (2004) 293–346.
- [3] P.K. Jain, X. Huang, I.H. El-Sayed, M.A. El-Sayed, Noble metals on the nanoscale: optical and photothermal properties and some applications in imaging, sensing, biology, and medicine, *Acc. Chem. Res.* 41 (2008) 1578–1586.
- [4] Y. Yin, A.P. Alivisatos, Colloidal nanocrystal synthesis and the organic-inorganic interface, *Nature* 437 (2005) 664–670.
- [5] T. Mokari, E. Rothenberg, I. Popov, R. Costi, U. Banin, Selective growth of metal tips onto semiconductor quantum rods and tetrapods, *Science* 304 (2004) 1787–1790.
- [6] H. Yu, M. Chen, P.M. Rice, S.X. Wang, R. White, S. Sun, Dumbbell-like bifunctional Au-Fe<sub>3</sub>O<sub>4</sub> nanoparticles, *Nano Lett.* 5 (2005) 379–382.
- [7] W. Shi, H. Zeng, Y. Sahoo, T.Y. Ohulchanskyy, Y. Ding, Z.L. Wang, M. Swihart, P. N. Prasad, A general approach to binary and ternary hybrid nanocrystals, *Nano Lett.* 6 (2006) 875–881.
- [8] Z. Xu, Y. Hou, S. Sun, Magnetic core/shell Fe<sub>3</sub>O<sub>4</sub>/Au and Fe<sub>3</sub>O<sub>4</sub>/Au/Ag nanoparticles with tunable plasmonic properties, *J. Am. Chem. Soc.* 129 (2007) 8698–8699.
- [9] W.-T. Chen, T.-T. Yang, Y.-J. Hsu, Au-CdS core-shell nanocrystals with controllable shell thickness and photoinduced charge separation property, *Chem. Mater.* 20 (2008) 7204–7206.
- [10] Z.-Q. Tian, Z.-L. Zhang, P. Jiang, M.-X. Zhang, H.-Y. Xie, D.-W. Pang, Core/shell structured noble metal (alloy)/cadmium selenide nanocrystals, *Chem. Mater.* 21 (2009) 3039–3041.
- [11] M. Li, X.F. Yu, S. Liang, X.N. Peng, Z.J. Yang, Y.L. Wang, Q.Q. Wang, Synthesis of Au-CdS Core-Shell Hetero-Nanorods with efficient Exciton-Plasmon interactions, *Adv. Funct. Mater.* 21 (2011) 1788–1794.
- [12] L. Wang, L. Wang, J. Luo, Q. Fan, M. Suzuki, I.S. Suzuki, M.H. Engelhard, Y. Lin, N. Kim, J.Q. Wang, Monodispersed core-shell Fe<sub>3</sub>O<sub>4</sub>@Au nanoparticles, *J. Phys. Chem. B* 109 (2005) 21593–21601.
- [13] S.-F. Hung, Y.-C. Yu, N.-T. Suen, G.-Q. Tzeng, C.-W. Tung, Y.-Y. Hsu, C.-S. Hsu, C.-K. Chang, T.-S. Chan, H.-S. Sheu, The synergistic effect of a well-defined Au@Pt core-shell nanostructure toward photocatalytic hydrogen generation: interface engineering to improve the Schottky barrier and hydrogen-evolved kinetics, *Chem. Commun.* 52 (2016) 1567–1570.
- [14] A.S. Zoofakar, R.A. Rani, A.J. Morfa, A.P. O'Mullane, K. Kalantar-Zadeh, Nanostructured copper oxide semiconductors: a perspective on materials, synthesis methods and applications, *J. Mater. Chem. C* 2 (2014) 5247–5270.
- [15] D. Snoke, J. Wolfe, A. Mysyrowicz, Quantum saturation of a Bose gas: excitons in Cu<sub>2</sub>O, *Phys. Rev. Lett.* 59 (1987) 827.
- [16] D. Gupta, S.R. Meher, N. Illyaskutty, Z.C. Alex, Facile synthesis of Cu<sub>2</sub>O and CuO nanoparticles and study of their structural, optical and electronic properties, *J. Alloys Compd.* 743 (2018) 737–745.
- [17] P.E. de Jongh, D. Vanmaekelbergh, J.J. Kelly, Cu<sub>2</sub>O: a catalyst for the photochemical decomposition of water, *Chem. Commun.* (1999) 1069–1070.
- [18] L. Zhang, D.A. Blom, H. Wang, Au-Cu<sub>2</sub>O core-shell nanoparticles: a hybrid metal-semiconductor heterostructure with geometrically tunable optical properties, *Chem. Mater.* 23 (2011) 4587–4598.
- [19] C.-H. Kuo, Y.-C. Yang, S. Gwo, M.H. Huang, Facet-dependent and Au nanocrystal-enhanced electrical and photocatalytic properties of Au-Cu<sub>2</sub>O Core-shell heterostructures, *J. Am. Chem. Soc.* 133 (2011) 1052–1057.
- [20] Y. Su, H. Guo, Z. Wang, Y. Long, W. Li, Y. Tu, Au@Cu<sub>2</sub>O core-shell structure for high sensitive non-enzymatic glucose sensor, *Sensor. Actuator. B Chem.* 255 (2018) 2510–2519.
- [21] L. Kong, W. Chen, D. Ma, Y. Yang, S. Liu, S. Huang, Size control of Au@Cu<sub>2</sub>O octahedra for excellent photocatalytic performance, *J. Mater. Chem.* 22 (2012) 719–724.
- [22] S.R. Manipaddy, A. Singh, B.M. Basavaraja, A.K. Samal, S. Srivastava, M. Saxena, Iron-Carbon hybrid magnetic nanosheets for adsorption-removal of organic dyes and 4-nitrophenol from aqueous solution, *ACS Applied Nano Materials* 3 (2020) 1571–1582.
- [23] S. Swain, B. M.B. V. Kandathil, P. Bhol, A.K. Samal, S.A. Patil, Controlled synthesis of palladium nanocubes as an efficient nanocatalyst for Suzuki-Miyaura cross-coupling and reduction of p-nitrophenol, *Langmuir* 36 (2020) 5208–5218.
- [24] M. Hong, L. Xu, F. Wang, S. Xu, H. Li, C.-z. Li, J. Liu, In situ synthesized Au-Ag nanocages on graphene oxide nanosheets: a highly active and recyclable catalyst for the reduction of 4-nitrophenol, *New J. Chem.* 40 (2016) 1685–1692.
- [25] J. Luo, Y. Gao, K. Tan, W. Wei, X. Liu, Preparation of a magnetic molecularly imprinted graphene composite highly adsorbent for 4-nitrophenol in aqueous medium, *ACS Sustain. Chem. Eng.* 4 (2016) 3316–3326.
- [26] V.K. Gupta, N. Atar, M.L. Yola, Z. Ustundag, L. Uzun, A novel magnetic Fe@Au core-shell nanoparticles anchored graphene oxide recyclable nanocatalyst for the reduction of nitrophenol compounds, *Water Res.* 48 (2014) 210–217.
- [27] K. Polat, M. Aksu, A. Pekel, Electroreduction of nitrobenzene to p-aminophenol using voltammetric and semipilot scale preparative electrolysis techniques, *J. Appl. Electrochem.* 32 (2002) 217–223.
- [28] N. Arora, A. Mehta, A. Mishra, S. Basu, 4-Nitrophenol reduction catalysed by Au-Ag bimetallic nanoparticles supported on LDH: homogeneous vs. heterogeneous catalysis, *Appl. Clay Sci.* 151 (2018) 1–9.
- [29] D. Leishangthem, M.A.K. Yumkhaibam, P.S. Henam, S. Nagarajan, An insight into the effect of composition for enhance catalytic performance of biogenic Au/Ag bimetallic nanoparticles, *J. Phys. Org. Chem.* 31 (2018), e3815.
- [30] Y.-Y. Wang, Y. Shu, J. Xu, H. Pang, Facile one-step synthesis of Ag@CeO<sub>2</sub> core-shell nanospheres with efficient catalytic activity for the reduction of 4-nitrophenol, *CrytEngComm* 19 (2017) 684–689.
- [31] X.H. Guo, J.Q. Ma, H.G. Ge, Synthesis and characterization of Cu<sub>2</sub>O/Au and its application in catalytic reduction of 4-nitrophenol, *Russ. J. Phys. Chem.* 89 (2015) 1374–1380.
- [32] R. Docampo, S.N. Moreno, The metabolism and mode of action of gentian violet, *Drug Metabol. Rev.* 22 (1990) 161–178.
- [33] A.M. Maley, J.L. Arbiser, Gentian Violet: a 19th century drug re-emerges in the 21st century, *Exp. Dermatol.* 22 (2013) 775–780.
- [34] S.M. Thomas, D.G. MacPhee, Crystal violet: a direct-acting frameshift mutagen whose mutagenicity is enhanced by mammalian metabolism, *Mutat. Res. Lett.* 140 (1984) 165–167.
- [35] M. Mittal, M. Sharma, O. Pandey, Photocatalytic studies of crystal violet dye using Mn doped and PVP capped ZnO nanoparticles, *J. Nanosci. Nanotechnol.* 14 (2014) 2725–2733.
- [36] T. Shende, B. Bhanvase, A. Rathod, D. Pinjari, S. Sonawane, Sonochemical synthesis of Graphene-Ce-TiO<sub>2</sub> and Graphene-Fe-TiO<sub>2</sub> ternary hybrid photocatalyst nanocomposite and its application in degradation of crystal violet dye, *Ultrason. Sonochem.* 41 (2018) 582–589.
- [37] J. Mittal, A. Malviya, V. Gupta, Adsorptive removal of hazardous anionic dye “Congo red” from wastewater using waste materials and recovery by desorption, *J. Colloid Interface Sci.* 340 (2009) 16–26.
- [38] J. Fowsiya, G. Madhumitha, N.A. Al-Dhabi, M.V. Arasu, Photocatalytic degradation of Congo red using Carissa edulis extract capped zinc oxide nanoparticles, *J. Photochem. Photobiol. B Biol.* 162 (2016) 395–401.
- [39] M.H. Habibi, M.H. Rahmati, The effect of operational parameters on the photocatalytic degradation of Congo red organic dye using ZnO-CdS core-shell nano-structure coated on glass by Doctor Blade method, *Spectrochim. Acta Mol. Biomol. Spectrosc.* 137 (2015) 160–164.
- [40] R.G. Saratale, G.D. Saratale, J.-S. Chang, S.P. Govindwar, Bacterial decolorization and degradation of azo dyes: a review, *Journal of the Taiwan Institute of Chemical Engineers* 42 (2011) 138–157.
- [41] L. Chen, F. Zhang, X.-Y. Deng, X. Xue, L. Wang, Y. Sun, J.-D. Feng, Y. Zhang, Y. Wang, Y.M. Jung, SERS study of surface plasmon resonance induced carrier movement in Au@Cu<sub>2</sub>O core-shell nanoparticles, *Spectrochim. Acta Mol. Biomol. Spectrosc.* 189 (2018) 608–612.
- [42] R. Costi, A.E. Saunders, U. Banin, Colloidal hybrid nanostructures: a new type of functional materials, *Angew. Chem. Int. Ed.* 49 (2010) 4878–4897.
- [43] J. Turkevich, P.C. Stevenson, J. Hillier, A study of the nucleation and growth processes in the synthesis of colloidal gold, *Discuss. Faraday Soc.* 11 (1951) 55–75.
- [44] M. Banerjee, S. Sharma, A. Chattopadhyay, S.S. Ghosh, Enhanced antibacterial activity of bimetallic gold-silver core-shell nanoparticles at low silver concentration, *Nanoscale* 3 (2011) 5120–5125.
- [45] R. Esparza, A. Santovena, A. Ruiz-Baltazar, A. Angeles-Pascual, D. Bahena, J. Maya-Cornejo, J. Ledesma-Garcia, R. Perez, Study of PtPd bimetallic nanoparticles for fuel cell applications, *Mater. Res.* 20 (2017) 1193–1200.
- [46] N.P.B. Tan, C.H. Lee, P. Li, Green synthesis of smart metal/polymer nanocomposite particles and their tuneable catalytic activities, *Polymers* 8 (2016) 105.
- [47] N.R. Jana, L. Gearheart, C.J. Murphy, Seed-mediated growth approach for shape-controlled synthesis of spheroidal and rod-like gold nanoparticles using a surfactant template, *Adv. Mater.* 13 (2001) 1389–1393.
- [48] R. He, Y.-C. Wang, X. Wang, Z. Wang, G. Liu, W. Zhou, L. Wen, Q. Li, X. Wang, X. Chen, Facile synthesis of pentacle gold-copper alloy nanocrystals and their plasmonic and catalytic properties, *Nat. Commun.* 5 (2014) 1–10.
- [49] F. Dong, W. Guo, S.-K. Park, C.-S. Ha, Controlled synthesis of novel cyanopropyl polysilsesquioxane hollow spheres loaded with highly dispersed Au nanoparticles for catalytic applications, *Chem. Commun.* 48 (2012) 1108–1110.

- [50] R. Jono, Y. Tateyama, K. Yamashita, A method to calculate redox potentials relative to the normal hydrogen electrode in nonaqueous solution by using density functional theory-based molecular dynamics, *Phys. Chem. Chem. Phys.* 17 (2015) 27103–27108.
- [51] Y. Won, L.A. Stanciu, Cu<sub>2</sub>O and Au/Cu<sub>2</sub>O particles: surface properties and applications in glucose sensing, *Sensors* 12 (2012) 13019–13033.
- [52] S. Shanmugam, P. Ulaganathan, S. Sivasubramanian, S. Esakkimuthu, S. Krishnaswamy, S. Subramaniam, *Trichoderma asperellum* laccase mediated crystal violet degradation-optimization of experimental conditions and characterization, *Journal of Environmental Chemical Engineering* 5 (2017) 222–231.
- [53] V.V. Chandanshive, N.R. Rane, A.S. Tamboli, A.R. Gholave, R.V. Khandare, S. P. Govindwar, Co-plantation of aquatic macrophytes *Typha angustifolia* and *Paspalum scrobiculatum* for effective treatment of textile industry effluent, *J. Hazard Mater.* 338 (2017) 47–56.
- [54] M. Pedroni, F. Piccinelli, T. Passuello, S. Polizzi, J. Ueda, P. Haro-Gonzalez, L. Martinez Maestro, D. Jaque, J. Garcia-Sole, M. Bettinelli, Water (H<sub>2</sub>O and D<sub>2</sub>O) dispersible NIR-to-NIR upconverting Yb<sup>3+</sup>/Tm<sup>3+</sup> doped MF<sub>2</sub> (M= Ca, Sr) colloids: influence of the host crystal, *Cryst. Growth Des.* 13 (2013) 4906–4913.